Journal of Inflammation Research

Dovepress
open access to scientific and medical research

Open Access Full Text Article

ORIGINAL RESEARCH

Genomic, Immunological, and Clinical Characterization of Pyroptosis in Ovarian Cancer

Min Zhou*
Bingshu Li*
Jianfeng Liu
Li Hong

Department of Gynecology and Obstetrics, Renmin Hospital of Wuhan University, Wuhan, Hubei, People's Republic of China

*These authors contributed equally to this work

Purpose: Pyroptosis is a form of lytic programmed cell death that is associated with the pathogenesis of many tumors. However, the potential roles of pyroptosis-related genes (PRGs) in the tumor microenvironment (TME) remain unclear.

Materials and Methods: We systematically described the genetic and transcriptional alterations in PRGs in gynecological cancers. An unsupervised clustering method was used to investigate the molecular subtypes of ovarian cancer (OV) and systematically analyze the TME cell infiltration characteristics. A prognostic signature and nomogram were established to quantify the pyroptosis patterns of individual tumors. We also analyzed the expression levels of eight PRGs in the OV tissues.

Results: Two distinct molecular subtypes of OV were identified, and these two distinct molecular subtypes could predict clinicopathological features, prognosis, TME stromal activity, immune infiltrating cells, and immune checkpoints. A prognostic signature was established, and its predictive capability was validated. Low risk score, characterized by activation of immunity, upregulation of programmed death-ligand 1 expression, lower tumor immune dysfunction and exclusion scores, lower tumor mutation burden, and favorable prognosis. These findings suggested that low-risk patients with OV may be more sensitive to immunotherapy. In addition, this signature could effectively predict the response to chemotherapy in patients with OV. Furthermore, a prognostic nomogram was generated, which exhibited superior predictive accuracy.

Conclusion: This study highlights the crucial role of PRGs in the TME and may help develop immunotherapies and promote individualized therapeutic strategies for patients with OV.

Keywords: pyroptosis, gynecological cancer, tumor microenvironment, immunotherapy, overall survival

Introduction

Pyroptosis is an inflammatory form of cell death that results in cell swelling, membrane lysis, chromatin fragmentation, and the release of pro-inflammatory factors.[1] It is believed to play a key role in eliminating various bacterial and viral infections.[2] Numerous studies have shown that in the absence of any bacterial or viral infection, it can chemically induce cell pyroptosis in cancer cells.[3] Pyroptosis can be induced through the non-canonical pathway involving caspase-4, 5, 11, and the canonical pathway of caspase-1 dependence. Many studies have focused on elucidating the molecular mechanism of pyroptosis in cancer cells, but the relationship between pyroptosis and cancer is complex and controversial, and the impact of pyroptosis on cancer varies with tissue and genetic background. Gasdermin D (GSDMD) is a pyroptosis executive protein that can be cleaved by inflammatory

Correspondence: Li Hong
Department of Gynecology and Obstetrics, Renmin Hospital of Wuhan University, No. 238, Jiefang Road, Wuhan, 430060, People's Republic of China
Tel/Fax +86 27-88041911
Email drhongli7777@gmail.com

Received: 15 October 2021
Accepted: 16 December 2021
Published: 24 December 2021

caspases and is essential for the secretion of interleukin-1β, making it a key mediator of inflammation.[4] The protein level of GSDMD was significantly elevated in non-small cell lung cancer (NSCLC) tissues and found to be linked to aggressive traits and worse prognosis.[5] GSDMD silencing suppressed cell proliferation, migration, and invasion, by inhibiting the EGFR/Akt signaling pathway and promoting apoptosis in NSCLC.[5] GSDME/DFNA5 (deafness, autosomal dominant 5), a member of the gasdermin family, has newly been identified as a promoter of pyroptosis upon its cleavage by caspase-3.[6] When GSDME is highly expressed, active caspase-3 cleaves it, causing release of its N-terminal domain, following which it punches holes in the cell membrane, causing the cells to swell, rupture, and die. Low expression of GSDME leads to the classic mechanism of tumor cell death, namely cell apoptosis.[7]

A growing number of studies have highlighted the potential effects of the tumor microenvironment (TME) on the development and progression of cancer.[8] Stroma sustains homeostasis and acts as a barrier to tumorigenesis under normal conditions. However, when a cell starts to become cancerous, the surrounding stroma changes to support tumor progression.[9] In addition to tumor cells, TME also consists of fibroblasts, endothelial cells, immune and inflammatory cells, extracellular matrix elements, as well as, diffusible cytokines and chemokines secreted from both cancer cells and stromal cells. The reciprocal crosstalk among these components eventually directs the development of the tumor. Emerging evidence also indicates crosstalk between pyroptosis and the TME.[10,11] At present, due to technical limitations, most studies focus on one or two pyroptosis-related genes (PRGs) and cell types, while in fact, the anti-tumor effect is characterized by numerous genes interacting in a highly coordinated manner. Hence, a comprehensive understanding of the characteristics of TME cell infiltration mediated by multiple PRGs may provide important insights for understanding the underlying mechanism of ovarian cancer (OV) tumorigenesis and predicting the response to immunotherapy.

In this study, we revealed global alterations of PRGs at transcriptional and genetic levels in three types of gynecological cancer, then evaluated the expression profiles of the PRGs, and obtained a comprehensive overview of the intratumoral immune landscape in 1003 OV samples from public datasets. First, 1003 patients with OV were stratified into two discrete subtypes, according to the PRGs. Based on the DEGs between the two subtypes, the patients were also divided into three gene subtypes. We further developed a scoring system to predict the overall survival (OS) and characterize the immune landscape of OV.

Materials and Methods

Data Source and Processing

Figure S1 shows a map of the process of the present work. The expression data, somatic mutation data, and corresponding clinical follow-up information from the gynecological tumor patient tissue datasets (TCGA-OV, TCGA-UCEC, and TCGA-CESC) were downloaded from UCSC. Three GEO OV chip datasets (GSE9891, GSE26712, and GSE49997) with survival times were selected from the GEO database. For the TCGA cohort, the fragments per kilobase million values were transformed into transcripts per kilobase million, as previously described. Four datasets were gathered, and the batch effect was eliminated using the "Combat" algorithm. Patients without complete survival information were excluded, and a total of 1003 OV patients were identified for further analysis.

Identification of Molecular Subtypes Based on PRGs

First, 25 PRGs were identified using MSigDB Team (REACTOME_PYROPTOSIS) (http://www.broad.mit.edu/gsea/msigdb/) and previous publications.[12] Full details of these genes have been given in Table S1. Next, k-means consensus clustering was carried out on the PRGs. The optimal cluster number distinguished the subtypes of OV, which is determined by clear separation of the consensus matrix heatmaps and cumulative distribution function (CDF) curves of the consensus score. Survival analysis and chi-square test or Fisher's exact test were used to compare the survival rates between the subtypes and determine the relationships between the clinicopathological parameters and clusters. Principal component analysis (PCA) was performed to downscale the sample data, to identify differences in distribution between subtypes. To investigate the differences in PRGs in terms of biological processes, GSVA was conducted with a hallmark gene set (C2 KEGG v.7.2) derived from the MSigDB database.

Immune Correlation Analysis

To identify the immune score-based relationships among molecular subtypes, we used the single-sample gene set enrichment analysis (ssGSEA) method of the GSVA package to score 23 immune cells and then compared the

differences in the immune scores among the molecular subtypes. The ESTIMATE algorithm was used to analyze the immune, stromal, and ESTIMATE scores for each sample. These scores represent the ratio of immune and stromal components to the total proportions of these components in the TME. Furthermore, the relationship between the two subtypes, based on PD-1 and PD-L1 expression, was also analyzed.

Identification and Functional Analysis of Differentially Expressed Genes (DEGs)

OV patients were divided into two pyroptosis subtypes, to identify PRGs. The limma package was used to identify the DEGs between two molecular subtypes, with the criteria of threshold false discovery rate <0.05, and |fold change| >1.5. Next, the intersecting genes for the two subtypes were identified, and KEGG pathway and GO functional enrichment analyses were conducted on the DEGs using the R package "Clusterprofiler".

Construction of the Pyroptosis-Related Prognostic Signature

A prognostic signature was constructed in three steps, as follows: 1) DEGs among the two molecular subtypes were processed using univariate Cox regression, to explore their associations with the OS of OV patients; 2) patients were classified into different groups (pyroptosis gene subtypes A, B, and C), for deeper analysis, using an unsupervised clustering method based on the expression of prognostic DEGs; 3) the entire cohort was randomly divided into training and validation groups at a cut-off of 1:1, following which the former was used to build a prognostic signature; 4) to minimize the risk of over-fitting, the least absolute shrinkage and selection operator (LASSO) Cox regression was applied; 5) following multivariable Cox regression analysis, genes with p-value <0.05, were regarded as independent prognostic factors of patient survival, and thus, utilized to construct a pyroptosis-related prognostic signature in the training set.

The risk value of signature was calculated as follows:

$$Risks\ Score = \Sigma(Expi * Coefi)$$

where Coefi and Expi denote the risk coefficient and expression of each gene, respectively. Risk scores of these genes for each patient were calculated on the basis of the coefficients of each gene in the Cox proportional hazards regression model, and categorized into low-risk and high-risk groups according to the median risk score. Kaplan–Meier survival curves were used to compare the OS between the two groups. The receiver-operating characteristic (ROC) curves of the risk score were plotted, and the area under the curve (AUC) was calculated to assess the performance of the risk score for prognosis prediction.

To evaluate the signature robustness in different datasets, the risk scores of each sample were calculated separately in the testing dataset and the other three GEO datasets (GSE9891, GSE26712, and GSE49997). Kaplan–Meier analysis was performed to show the survival difference between the high- and low-risk groups. An AUC analysis was performed to evaluate the predictive performance of the model.

Acquisition of Tissues

Five OV and nearby non-tumor tissues were harvested from patients with OV at the Renmin Hospital of Wuhan University. The samples were preserved at −80°C until use. Written informed consent was obtained from all the individuals included in this study. The study was approved by the Ethics Committee of the Renmin Hospital of Wuhan University.

RNA Isolation and Quantitative Real-Time Polymerase Chain Reaction (qRT-PCR)

Total RNA from tissues of OV patients was extracted using RNAiso Plus (9108, TaKaRa, Japan), according to the manufacturer's protocol. Following that, the Hifair II 1st Strand cDNA Synthesis SuperMix Kit (11123ES10,Yeasen, Shanghai, China) was used for reverse transcription of cDNA. qRT-PCR was conducted using Hieff qPCR SYBR Green Master Mix (11201ES03, Yeasen). GAPDH was used as an endogenous control for mRNA expression. Expression level analysis was performed using the $2^{-\Delta\Delta Ct}$ method. All primer sequences used in this study are listed in Table S2.

Clinical Correlation Analysis of the Prognostic Signature

Associations between the clinical parameters and risk score were evaluated using chi-square and Wilcoxon tests, and have been represented in heatmaps. Univariate and multivariate analyses were performed to assess the independent prognostic value of risk scores and clinical parameters, including age, FIGO stage, grade, histological subtype, and tumor status. A stratified analysis was carried out based on

the clinical parameters of the patients, including age, FIGO stage, grade, histological subtype, and tumor status.

Evaluation of Immune Landscape Between the Two Groups

To reveal the relationship between the prognostic risk signature and immune cell infiltration, ssGSEA was used to quantify the relative infiltration of 23 immune cells. Differences between the two groups were assessed using the Kruskal–Wallis test, and the results are shown as a boxplot. We also analyzed the association between the fractions of 23 immune cells and the eight genes in the signature. Moreover, the signature was comprehensively analyzed to determine its relationship with immune checkpoints in OV. Because immune checkpoint inhibitors (ICIs) can enhance anticancer immunity, we predicted the potential response of ICIs using the tumor immune dysfunction and exclusion (TIDE) algorithm.[13]

Mutation and Drug Susceptibility Analyses

To identify somatic mutations in patients with OV, we downloaded single-nucleotide polymorphism data and clinical follow-up information from the TCGA database. The downloaded single-nucleotide polymorphism data were organized in the multiple alignment format and visualized using the "maftools" package in R software. The horizontal histogram shows the genes with the highest frequency of mutations. The tumor mutation burden (TMB; mutations per million bases) of each patient was calculated, and the TMB levels between the two groups were compared using the Wilcoxon test. A chi-square test was conducted to identify the genes that were significantly differentially mutated between the high- and low-risk groups. To explore differences in therapeutic effects of chemotherapeutic drugs in patients across the high- and low-score groups, we calculated the semi-inhibitory concentration (IC_{50}) values of chemotherapeutic drugs commonly used to treat OV using the "pRRophetic" package.

Establishment of a Predictive Nomogram

Based on the risk scores and clinicopathological characteristics, the R package "rms" was employed to establish a prognostic nomogram. The prognostic accuracy of the nomogram was estimated in terms of the AUC and depicted by means of ROC curves. Calibration curves of the nomogram were used to examine the concordance between the predicted and observed survival.

Results

Genetic and Transcriptional Alterations of PRGs in Gynecological Cancer

A total of 25 PRGs were included in the present study. We summarized the incidence of somatic mutations in 25 PRGs and showed the highest mutation frequency of PRGs in the OV cohort (91.06%; Figure 1A), followed by the UCEC (53.69%; Figure 1B) and CESC cohorts (17.65%; Figure 1C). Among these three gynecological tumors, the mutation frequency of TP53 was the highest. In the OV cohort, the mutation frequency of TP53 was 90% (Figure 1A). Next, we investigated the somatic copy number alterations in these PRGs and observed a prevalent copy number alteration in 25 PRGs. We observed extensive copy number variation (CNV) deletions in the UCEC cohort (Figure 1D), while the ratios of copy number gain and deletion in the OV (Figure 1E) and CESC cohorts (Figure 1F) were similar. Among them, PRKACA, TNF, and AIM2 had widespread CNV gains in the three cohorts, while GPX4 and CASP9 presented CNV loss. Figure 1G–I shows the location of CNV alterations in the PRGs on chromosomes. To clarify whether the expression levels of PRGs in patients with gynecological tumors are affected by these genetic variants, we compared the mRNA expression levels between normal tissues and tumor tissues and found that there was no significant correlation between the expression levels of PRGs and CNV alterations (Figure 1J–L). Considering the significant difference in PRG expression between OV and normal tissues and the relatively comprehensive clinical records, we selected the OV cohort for subsequent analysis.

Identification of Pyroptosis Subtypes in OV

To fully understand the expression pattern of PRG involved in tumorigenesis, 1003 patients from four eligible OV cohorts were integrated into our study for further analysis; the detailed clinicopathological information of the patients is shown in Table S3. Univariate Cox regression and KM analyses indicated the prognostic significance of the 25 PRGs (Table S4). The comprehensive landscape of PRG interactions, regulator connections, and their prognostic value for OV patients was demonstrated by means of a pyroptosis network (Figure 2A and Table

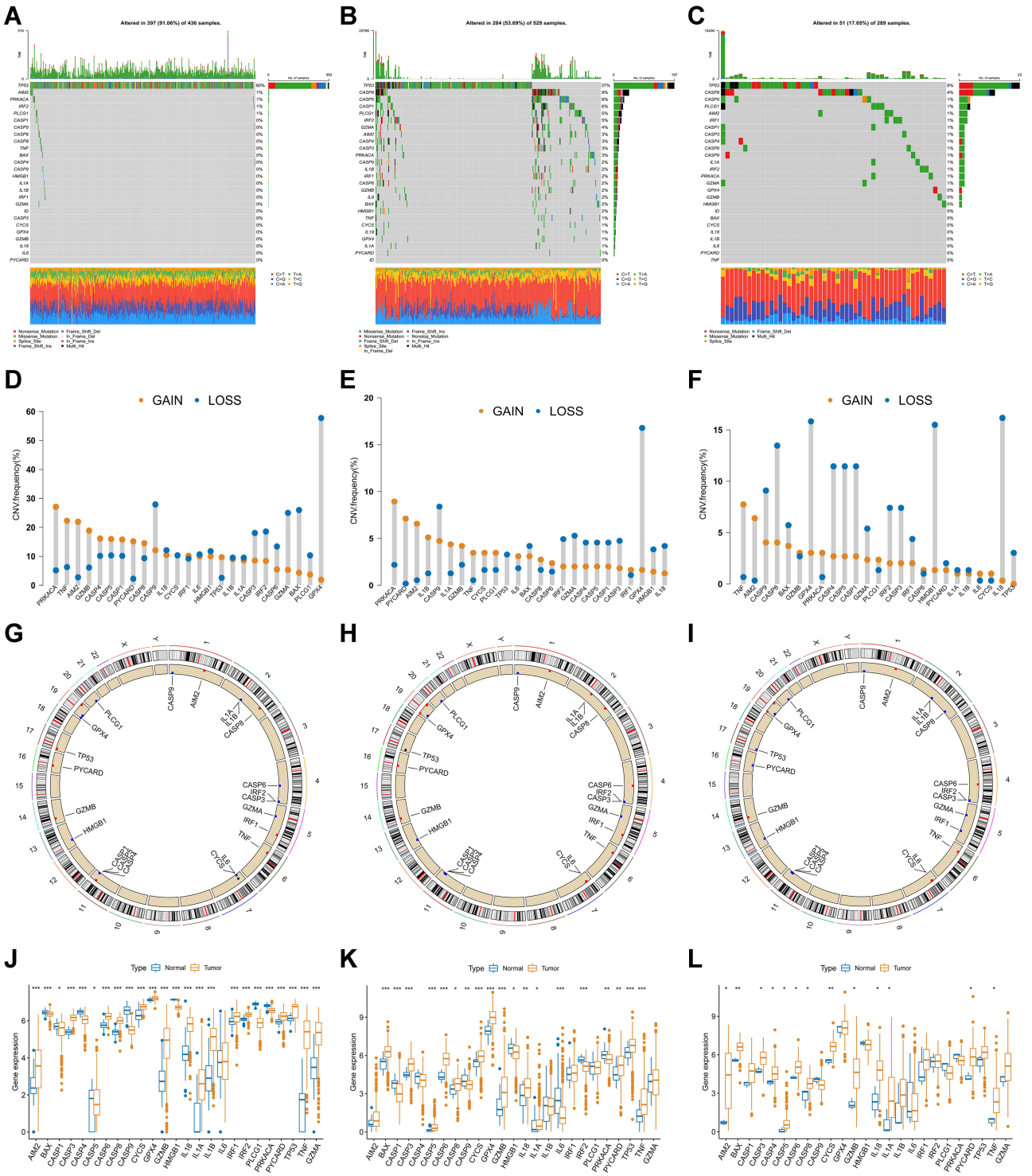

Figure 1 Genetic and transcriptional alterations of pyroptosis-related genes in gynecological tumors. (**A**–**C**) The mutation frequency of 25 pyroptosis-related genes in OV, UCEC, and CESC cohorts. (**D**–**F**) The frequency of CNV change of pyroptosis-related genes in OV, UCEC, and CESC cohorts. (**G**–**I**) The location of CNV alterations in pyroptosis-related genes on 23 chromosomes. (**J**–**L**) The expression distribution of 25 pyroptosis-related genes in normal and gynecological cancer tissues. *p<0.05, **p<0.01, and ***p<0.001.

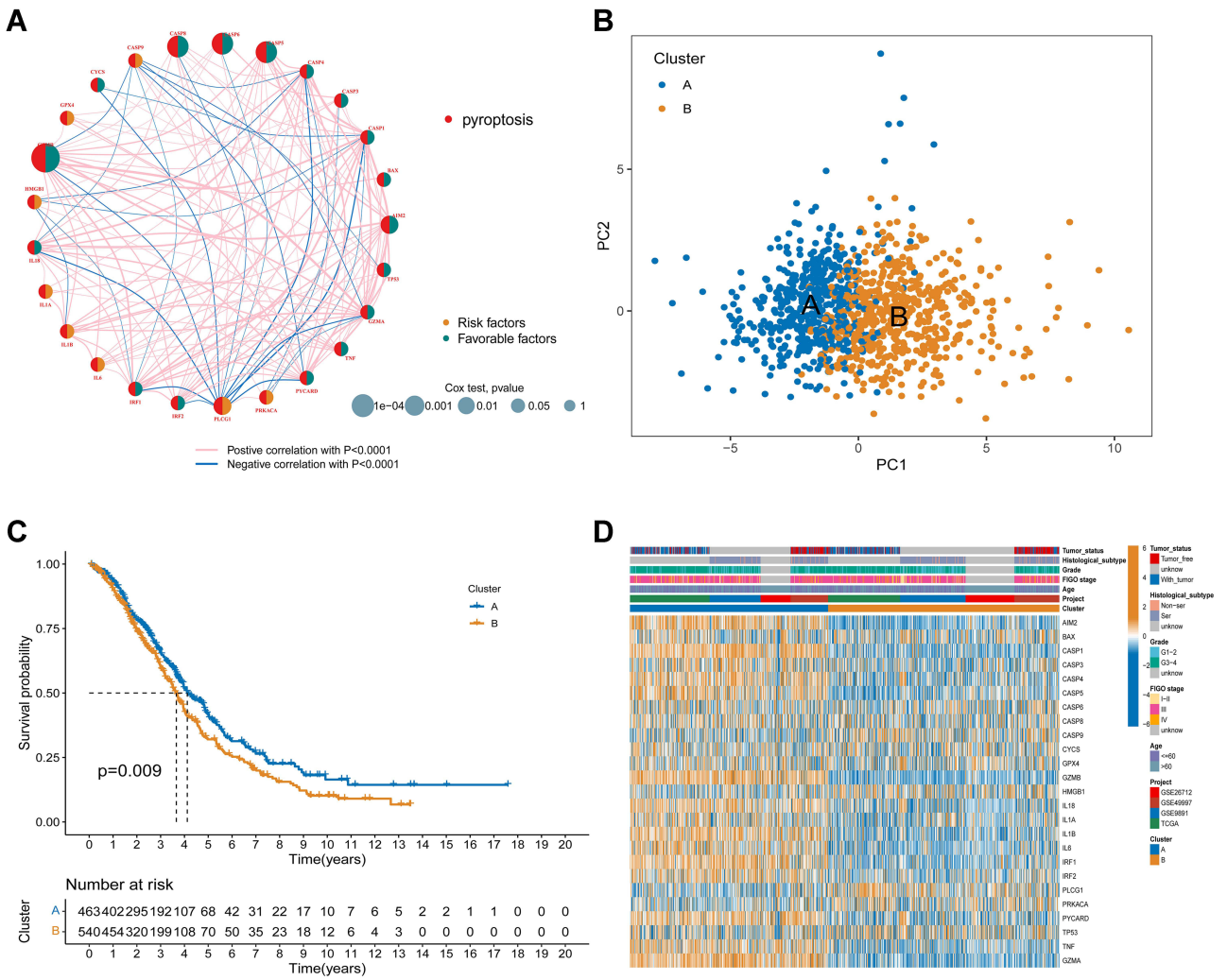

Figure 2 Identification of pyroptosis subtypes in ovarian cancer. (**A**) The interactions among PRGs in OV. The line connecting the PRGs represents the interaction between them. A blue line represents a negative correlation, while a pink line represents a positive correlation. (**B**) Principal component analysis showed that the two subtypes were different. (**C**) Kaplan–Meier curves of the OS between the two pyroptosis subtypes. (**D**) Comparison of the distribution of patients with different clinicopathological features between the two pyroptosis subtypes.

S5). To further investigate the expression characteristics of PRGs in OV based on the expression profile of the 25 PRGs, we performed k-means consensus clustering for 1003 patients from k=2 to k=9, based on the expression similarity of the PRGs (Figure S2); it appeared that k=2 was the optimal selection. The results were most reliable and stable when patients with OV were divided into two subtypes with 463 patients in cluster 1 and 540 patients in cluster 2. PCA showed that the two subtypes could be different (Figure 2B). Kaplan–Meier analysis showed that patients with subtype A had a longer OS than their counterparts with subtype B (Figure 2C). Figure 2D shows the relationships between the two subtypes, revealing a distinct difference between the subtypes in terms of clinicopathological features. Thus, the results of the consensus clustering analysis were associated with the progression of OV and survival of patients with OV.

Immune Landscape of Distinct Subtypes in OV

GSVA enrichment analysis showed that subtype A was significantly enriched in immune-activation pathways, including natural killer cell-mediated cytotoxicity, T and B cell receptor signaling pathway, activation of the chemokine signaling pathway, cytokine-cytokine receptor interaction, as well as, NOD-like and Toll-like receptor signaling pathways (Figure 3A and Table S6). To estimate the association between the two subtypes and the TME, the ESTIMATE algorithm was employed

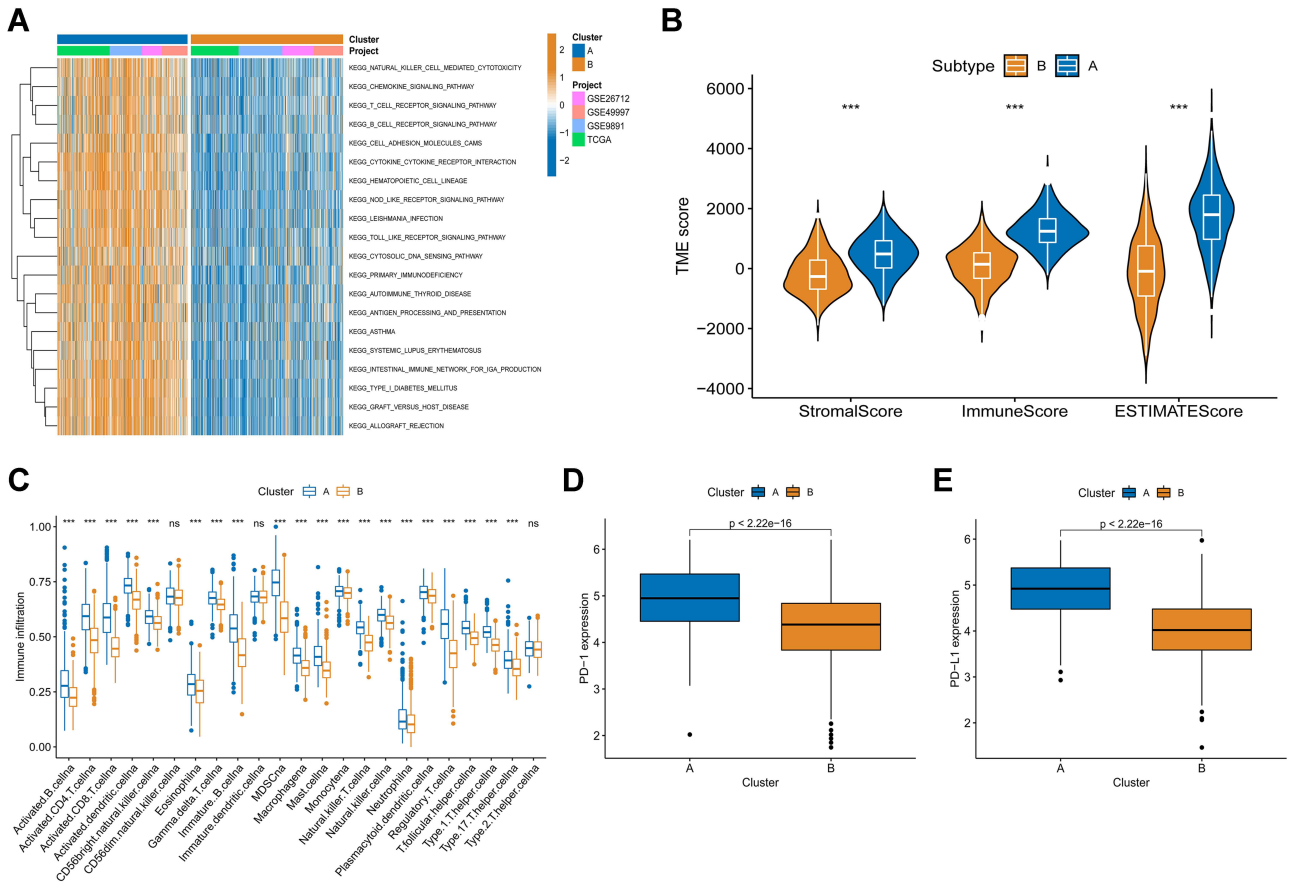

Figure 3 Immune landscapes of the two subtypes of ovarian cancer. (**A**) Differences in pathway activities between the two distinct subtypes, as scored using GSVA. (**B**) The relationship between TME score and the two subtypes. (**C**) Comparison of the relative abundance of infiltrating immune cells between the two subtypes. (**D** and **E**) Comparison of the expression level of PD-l and PD-L1 between the two subtypes. ***p<0.001, ns, not significant.

to obtain the immune, stromal, and ESTIMATE scores (Table S7). Based on the Wilcoxon rank-sum test, we found a significant difference between the scores for subtypes A and B (Figure 3B). The relative fractions of 23 tumor-infiltrating immune cells (TIICs) were calculated using the ssGSEA algorithm (Table S8). Subtype B exhibited a decreased abundance of TIICs, such as activated B cells, $CD4^+$/$CD8^+$ T cells, and natural killer cells, which play a vital role in anti-tumor immunity (Figure 3C). Taken together, the expression of PRGs in the subtypes might have immunomodulatory effects on the TME. Given this, we attempted to determine the correlation between the subtypes and two important immune checkpoints and showed higher PD1 and PD-L1 expression in subtype A (Figure 3D and E).

Identification of Gene Subtypes Based on DEGs in OV

To further explore the potential biological behavior of each subtype of pyroptosis, we identified 349 pyroptosis subtype-related DEGs using the R package "limma", and performed functional enrichment analysis (Figure 4A and B and Table S9). Interestingly, these DEGs were significantly enriched in biological processes that were significantly related to immunity (Figure 4A). KEGG analysis revealed that inflammation and immune-related pathways were highly enriched (Figure 4B), suggesting that pyroptosis plays a non-negligible role in the immune regulation of the TME. We then conducted univariate analysis to identify the prognostic role of 349 subtype-related genes, following which 107 prognosis-related genes were screened out and used for subsequent analysis (Table S10). To further validate this regulation mechanism, a consensus clustering algorithm was used to divide the patients into three genomic subtypes, based on prognostic genes: gene subtypes A-C (Figure S3). Patients with gene subtype B had the worst OS, whereas patients with gene subtype A presented favorable OS (Figure 4C). In addition, analysis of the expression of PRGs and clinical features of the three gene subtypes revealed significant differences between the three

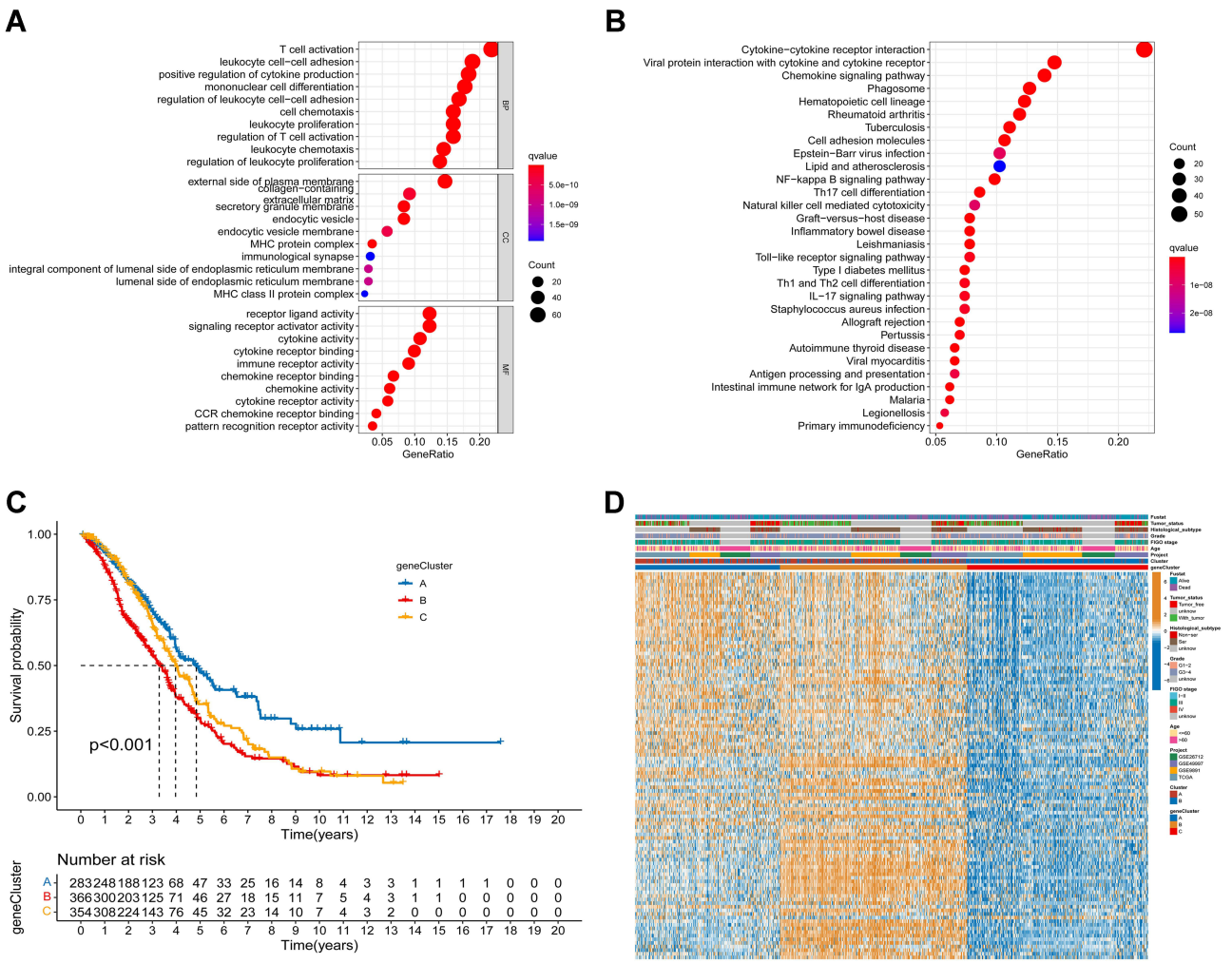

Figure 4 Identification of gene subtypes in ovarian cancer, based on DEGs. (**A** and **B**) Functional enrichment analyses of DEGs between the two pyroptosis subtypes. (**C**) Kaplan–Meier curves for OS of the three gene subtypes (p<0.001). (**D**) Comparison of the distribution of patients with different clinicopathological features between the three gene subtypes.

gene subtypes in terms of expression of PRGs, FIGO stage, grade, histological subtype, tumor status, and survival status (Figure 4D).

Establishment and Evaluation of the Prognostic Signature in OV

A prognostic scoring system was constructed based on these subtype-related prognostic genes. Figure 5A shows the distribution of patients in the two pyroptosis subtypes, three gene subtypes, and two risk score groups. We randomly divided 1003 patients with OV into training (n=503) and testing (n=500) sets. Following LASSO regression analysis, 25 genes remained according to the minimum partial likelihood deviance (Figure 5B and C). An optimum prognostic signature involving eight genes (SLC31A2, LYN, CD44, EPB41L3, VSIG4, FCN1, IRF4, and ISG20) was ultimately defined based on stepwise multivariate Cox regression analysis. Risk score = (0.347 × SLC31A2 expression) + (−0.368 × LYN expression) + (−0.377 × CD44 expression) + (0.432 × EPB41L3 expression) + (0.280 × VSIG4 expression) + (−0.251 × FCN1 expression) + (−0.240 × IRF4 expression) + (−0.200 × ISG20 expression). Next, we calculated the risk score of each sample and observed a significant difference in the risk score between pyroptosis gene subtypes. The risk score of subtype A was the lowest, and the risk score of subtype B was the highest, indicating that low-risk score may be closely related to immune activation-related features, while high-risk score may be related to immune inhibition-related features (Figure 5D). More importantly, as compared to subtype A, subtype B had a significantly higher risk score

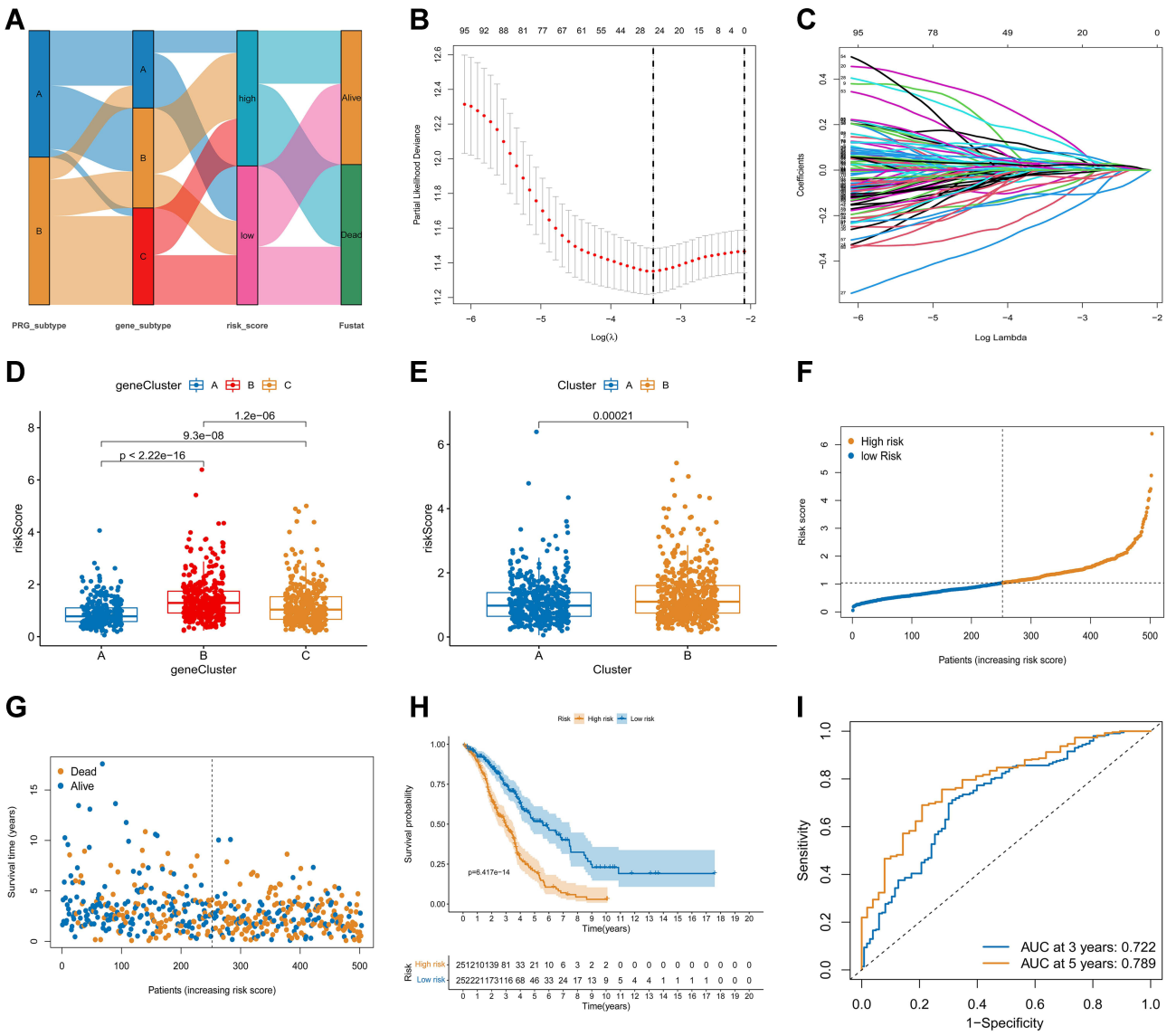

Figure 5 Construction of prognostic signature for patients with ovarian cancer in the training set. (**A**) Alluvial diagram for distribution of pyroptosis subtypes in groups with different gene subtypes, risk scores, and survival outcomes. (**B**) Cross-validation for optimal penalty parameter selection in the LASSO model. (**C**) LASSO coefficient profiles of 25 prognostic genes. (**D**) The difference in risk score between the gene subtypes. (**E**) The difference in risk score between the pyroptosis subtypes. (**F** and **G**) The distribution and scatter plots of the risk score. (**H**) Kaplan–Meier curves of the OS between the different risk groups. (**I**) ROC curves of the signature to predict 3- and 5-year survival.

(Figure 5E). The risk score distribution of the training set is shown in Figure 5F and G. The figure indicates that the risk of death of a patient with a high-risk score sample was significantly higher than that of a patient with a low-risk score sample. Similarly, the Kaplan–Meier curves revealed a higher chance of death in the high-risk group than that in the low-risk group (Figure 5H). To assess the predictive ability of the signature, ROC curves for 3-year and 5-year survival were created, which exhibited AUC values of 0.722 and 0.789, respectively (Figure 5I), indicating preferable sensitivity and specificity.

To validate the robustness of the model, we calculated the risk score in the testing set and other 3 GEO data sets (GSE9891, GSE26712, and GSE49997), and the results showed that the risk score distribution was consistent with that of the training set and higher risk scores also indicated worse OS (Figure S4A–D). Kaplan–Meier survival analysis demonstrated that the high-risk group exhibited

a significantly poorer prognosis than the low-risk group (Figure S4E–H). The ROC curves indicated that the signature showed promising performance in predicting the OS of OV patients (Figure S4I–L).

Expression Levels of the Eight PRGs That Constitute the Prognostic Signature in OV Tissues

Expression levels of the eight prognostic PRGs were measured in five OV tissues and adjacent normal tissues using RT-qPCR. As shown in Figure S5, VSIG4, CD44, IRF4, EPB41L3, and SLC31A2 were elevated in OV tissues, and ISG20, FCN1, ICOS, and LYN were downregulated in OV tissues, as compared to the corresponding normal tissues.

Clinical Correlation Analysis of the Prognostic Signature

To further verify the significance of the prognostic signature in clinical practice, we examined the correlation between the prognostic signature and the available clinical characteristics of OV. We observed that higher risk scores in patients were significantly associated with advanced-stage, serous histological subtype, and tumor status ($p<0.05$; Figure S6A–C). To determine whether this prognostic risk score might independently predict the OS for OV patients, we performed univariate and multivariate Cox regression analyses in the entire cohort by incorporating the factors of age, FIGO stage, histological subtype, grade, tumor status, and risk score. The results suggested that age, FIGO stage, tumor status, and risk score can independently predict the prognosis of patients with OV (Figure S6D–E). A stratified analysis was carried out based on the clinicopathological characteristics of the patients, including age, FIGO stage, grade, histological subtype, and tumor status. Patients could be divided into significantly different low- and high-risk groups according to all these variables, which further indicated that our model still had good predictive power in different clinical subgroups (Figure S7).

Evaluation of the Differential Immune Landscape Between the High- and Low-Risk Groups

Due to the strong association between clinicopathology and TME immune activity, we comprehensively investigated the correlation between the risk score and the abundance of immune cells using the ssGSEA algorithm. The results demonstrated that infiltration of activated B cells and $CD4^+$ and $CD8^+$ T cells increased in the low-risk group, while regulatory T cells and follicular helper T cells associated with poor prognosis had a higher proportion in the high-risk group (Figure 6A). Spearman correlation analysis showed a strong correlation between the eight genes in the model and most of the immune cells (Figure 6B). These results indicated that these eight genes play a critical role in immune infiltration and might have significant clinical value in patients with OV. In addition, we analyzed the correlation between immune checkpoints and the risk model developed in this study. Figure 6C shows that 30 immune checkpoints were differentially expressed in the two groups, including PD-1, PD-L1, and CTLA-4. Furthermore, the TIDE algorithm was used to predict the likelihood of response to immunotherapy. Interestingly, we found that low-risk patients may be more sensitive to immunotherapy than high-risk patients (Figure 6D).

Mutation and Drug Susceptibility Analyses

We explored the differences in somatic mutations between the high- and low-risk groups based on the TCGA-OV cohort (Figure 7A and B). Waterfall plots depicted the frequently mutated genes in OV stratified by high- and low-risk groups. The top three mutated genes were TP53, TTN, and MUC16. Although the high- and low-risk groups had similar somatic mutations (92.42% vs 92.68%), the mutation frequencies of TP53, TTN, MUC16, and CSMD3 were significantly different. Next, we estimated the relationship between the signature and TMB. The results indicated that the TMB ($p=0.003$; Figure 7C) in the low-risk group was lower than that in the high-risk group. To evaluate the influence of TMB on the survival of OV patients, all patients were categorized into low- and high-TMB groups, based on the optimal cut-off value determined by the "survminer" package in R. The results demonstrated that patients with high TMB had prolonged survival ($p=0.019$; Figure 7D). The subsequent stratified survival analysis showed that the risk score could distinguish the survival of OV patients in both high- and low-TMB subgroups, and the trend of survival advantage in the high-TMB group was reversed by the risk score (Figure 7E). Our results proved that for patients with OV, the risk score is an effective and robust prognostic factor independent of TMB, and different genetic mutation landscapes exist in the two risk groups. We then selected chemotherapy drugs that are currently used for the

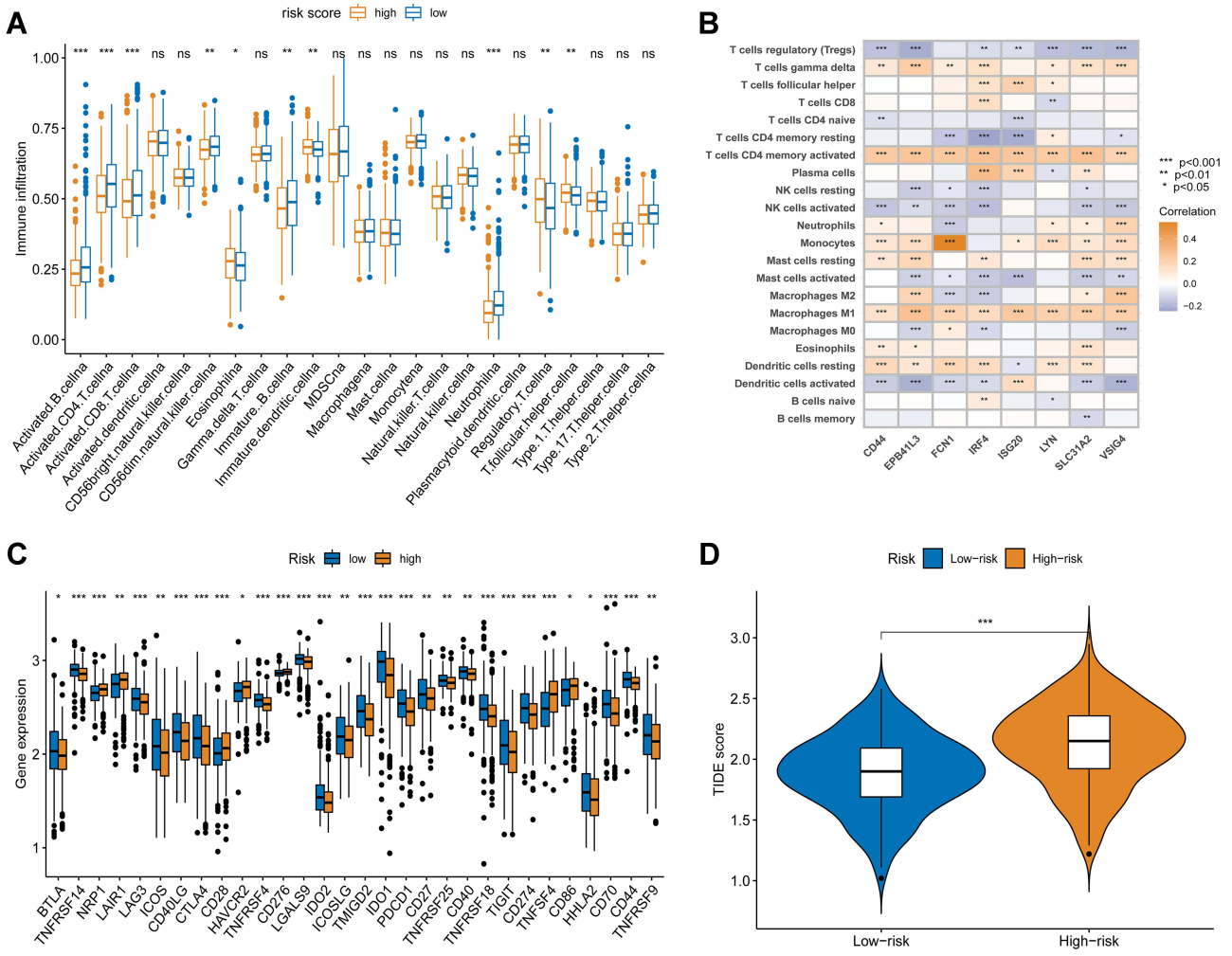

Figure 6 Evaluation of the immune landscape between the high- and low-risk groups. (**A**) Correlation of risk score and immune cell types. (**B**) Correlation of immune cell infiltration and the eight genes in the proposed model. (**C**) Differential expression of immune checkpoints in the two risk groups. (**D**) Distribution of TIDE scores in high- and low-risk groups. *p<0.05, **p<0.01, and ***p<0.001, ns, not significant.

treatment of OV, and evaluated the sensitivity of patients in the two groups to these drugs. Patients in the high-risk group had lower IC_{50} values for chemotherapy drugs, such as cisplatin, docetaxel, doxorubicin, and elesclomol, while patients in the low-risk group might be more susceptible to treatment with gemcitabine, paclitaxel, and gefitinib. Together, these results showed that PRGs were related to drug sensitivity (Figure 7F–L).

Development of a Nomogram for Predicting Survival

To improve the clinical power of the signature, we established a nomogram to predict 3- and 5-year survival rates in OV.e, according to the algorithm (Figure 8A). The AUC of the nomogram for predicting the 3- and 5-year survival times in the whole cohort were 0.730 and 0.785, respectively (Figure 8B), while the 3- and 5-year AUC values of the nomogram in an external cohort (GSE9891) were 0.771 and 0.722, respectively (Figure 8C). Subsequently, calibration plots were established in the whole cohort, as well as, the external cohort, which suggested that in comparison to an ideal model, the proposed nomogram had a similar performance (Figure 8D and E).

Discussion

A growing number of studies have revealed a crosstalk between pyroptosis and anti-tumor immunity.[14,15] Although most studies have focused on a single PRG or a single type of TME cell, the overall effect and TME infiltration characteristics mediated by the combined effects of multiple PRGs have not yet been fully recognized. In the present study based on the

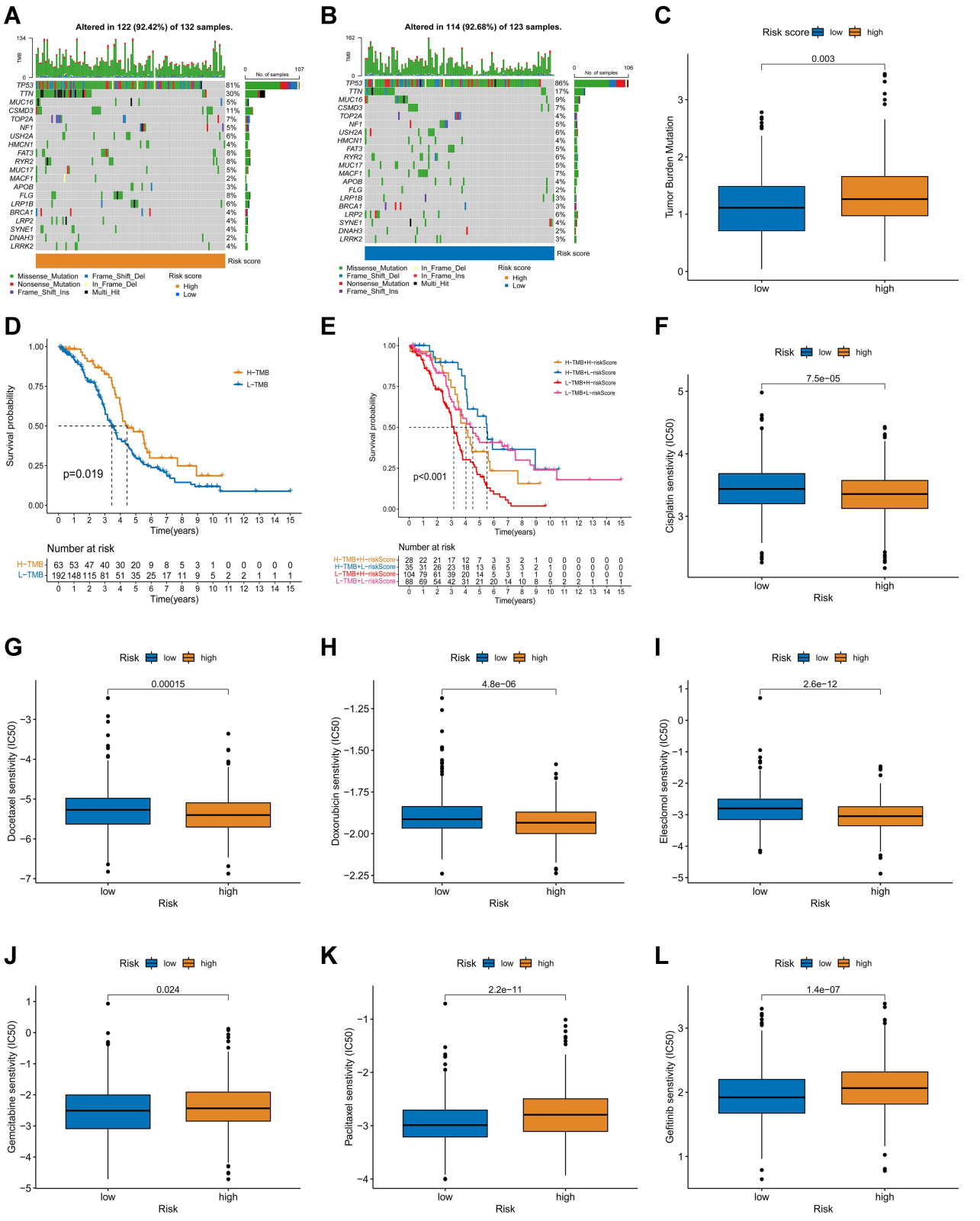

Figure 7 Comparison of the mutation and drug susceptibility between the two risk groups of ovarian cancer. (**A** and **B**) Waterfall plot of somatic mutation features in the high-risk (**A**) and low-risk (**B**) groups. Each column represents an individual patient. The mutation frequency is listed in the upper bar chart, and the proportion of each mutation type is shown in the bar graph on the right. (**C**) Difference in TMB levels between the high- and low-risk groups. (**D**) Survival analysis between the high- and low-TMB groups. (**E**) Survival analysis among patients stratified by risk score and TMB. (**F**–**L**) The IC_{50} values of seven chemotherapy drugs between the high- and low-risk groups. Cisplatin (**F**), docetaxel (**G**), doxorubicin (**H**), elesclomol (**I**), gemcitabine (**J**), paclitaxel (**K**), and gefitinib (**L**).

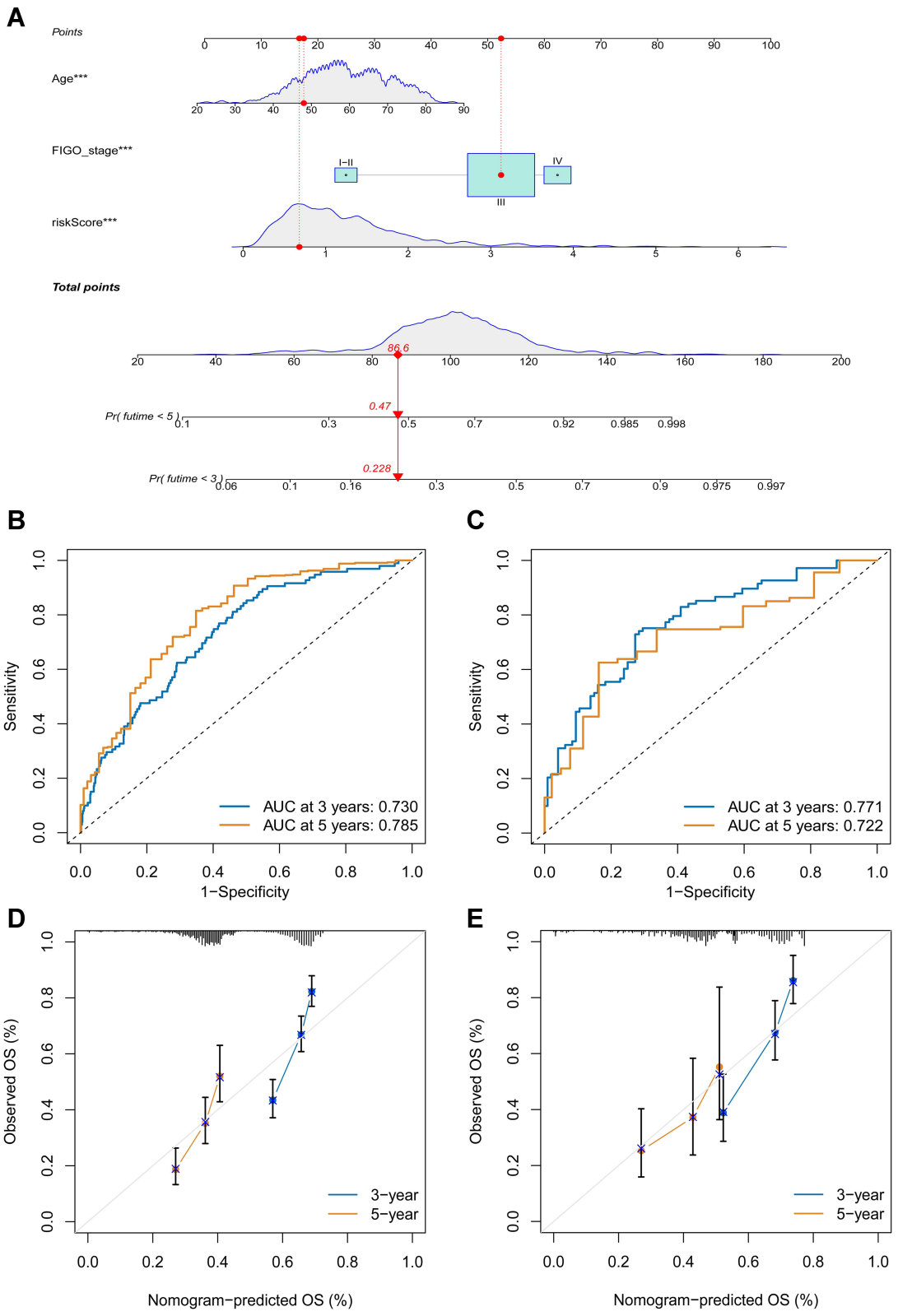

Figure 8 Establishment of a prognostic nomogram for ovarian cancer. (**A**) A nomogram for integration of clinicopathological parameters and risk score in the whole set. (**B** and **C**) ROC curves for predicting the 3- and 5-year survival ROC curves in the whole and external sets. (**D** and **E**) Calibration curves of the pyroptosis-clinical nomogram in the whole and external sets. Calibration curves depict the calibration of the pyroptosis clinical nomogram in terms of the agreement between the predicted 3- and 5-year overall survival and observed outcomes. ***p<0.001.

PRGs were further identified by means of consensus clustering. The two subtypes exhibited significantly distinct clinical features, immune status, biological processes, and outcomes. The OV subtype is also characterized by significant immune-related biological pathways. To further verify this regulation mechanism, a consensus clustering algorithm was used to categorize patients into three genomic clusters, according to the prognostic DEGs between the two pyroptosis subtypes. These findings suggested that PRGs might serve as prognostic biomarkers for estimating the clinical outcome and immunotherapy response of OV. Therefore, we combined LASSO regression and multivariate Cox regression analysis to screen for the most informative prognostic indicators that could compose the final signature. Ultimately, we derived a prognostic risk signature that showed favorable predictive ability. The expression levels of the eight genes in the model were also explored experimentally in OV tissues. The pyroptosis pattern characterized by immune inhibition presented a higher risk score, whereas the pattern characterized by immune activation presented a lower risk score. Patients divided by risk score into low- and high-risk score groups exhibited significantly different clinicopathological characteristics, prognosis, mutation, TME, immune checkpoints, response to immunotherapy, and drug susceptibility. High-risk scores in patients were significantly associated with advanced-stage, serous histological subtype, tumor status, and poor prognosis, suggesting that it exhibits satisfactory clinical utility, which might improve prognostic predictions of survival risks and lead to the creation of additional clinical therapies. A low-risk score was characterized by activation of immunity, upregulation of PD-L1 expression, lower TIDE scores, lower TMB, and a favorable prognosis. These findings suggested using multivariate Cox regression analysis, a nomogram was constructed, which demonstrated superior predictive accuracy. Based on the total points calculated by the nomogram, clinicians may recommend certain courses of action. For example, the guidelines could suggest that patients with poorly differentiated histology should undergo palliative chemotherapy because of their low life expectancy. On the other hand, patients with well-differentiated histology have a better prognosis, so debulking surgery could be chosen in their case. However, solely depending on the TNM classification for patient selection may be ambiguous and doctors would have to rely on their clinical experience. Using the nomogram proposed in this study, oncologists would be in a better position to select patients with better survival rates, because they would have a higher probability of benefiting from palliative resection, as it consists of a larger combination of clinicopathological parameters. Thus, using a nomogram to identify subgroups of patients with a more homogeneous prognosis, physicians can assess a diverse range of parameters with more objectiveness and precision for OV, so that the interpretation of clinical trial outcomes becomes clearer. The nomogram can also be used to assess individual clinical outcomes and the potential for specific OV treatments.

OV is one of the main causes of death from gynecological malignancies. Although progress has been made in the treatment of OV, most patients relapse after first-line treatment, depending on the tumor and non-tumor heterogeneity of the tumor and surrounding TME. The TME in OV is a crucial orchestrator of OV progression, and therefore, should be considered as a necessary target of combination therapy. Substantial heterogeneity exists across patients with OV, which contributes to differential clinical outcomes and highlights the crucial role of the TME in OV tumorigenesis and progression.[16–18] There is increasing evidence regarding the clinical significance of the TME in the context of predicting tumorigenesis, progression, prognosis, and therapeutic efficacy in various cancers.[8,19,20] The typical structure of the TME comprises of immune and inflammatory cells, endothelial cells, myofibroblasts, fibroblasts, adipose cells, and the extracellular matrix.[9] In this study, we conducted a thorough analysis of the association between the signature and TME immune activity. The results showed a significant difference between the pyroptosis subtypes A and B. GSVA enrichment analysis showed that subtype A was significantly enriched in e immune pathways and showed a higher risk score. Additionally, we discovered that characteristics of the TME and the abundance of 23 TIICs were different between the two molecular subtypes, implying the vital role of PRGs in OV progression. Specifically, OV is an immunogenic tumor with a spontaneous anti-tumor immune response. Lymphocyte infiltration in tumor biopsy samples has been associated with improved survival of patients with a range of cancers, including melanoma.[21] Tumor-infiltrating T cells, especially $CD4^+$ and $CD8^+$ T cells, are present in the ovarian TME and are closely associated with a good prognosis. In the subset of high-grade serous OV, tumors harboring BRCA1/2 mutations demonstrate a higher neoantigen burden, as well as $CD3^+$ and $CD8^+$ tumor-infiltrating lymphocytes. Increased levels of PD-1 and PD-L1 expression on TIICs, as compared to that in homologous recombination-proficient tumors indicates that PD-1/PD-L1 inhibitors may be more effective in BRCA1/2-mutated tumors than in homologous

recombination-proficient tumors.[22] Several studies have demonstrated that a high density of $CD8^+$ T cells predicts a relatively favorable signal for the prognosis of OV patients.[23,24] Although $CD4^+$ T cells are generally non-cytotoxic, they can help recruit and activate $CD8^+$ T toxic lymphocytes and enhance their anti-tumor immune effects. Some studies have demonstrated that the densities of tumor-infiltrating $CD4^+$ T cells in OV tissues are higher, and higher densities indicate a good prognosis.[23] In this study, subtype A and low-risk scores, with a favorable prognosis, showed higher immune infiltration of activated $CD4^+$ and $CD8^+$ T cells, suggesting that they play an active role in the tumorigenesis and progression of OV. As the predominant antigen-presenting cells, dendritic cells (DCs) play an antigen-presenting role in activating T cells and natural killer cells,e.[25] Our results suggest insufficient DC infiltration in subtype B and high-risk score groups. A recent prospective study revealed that patients with high infiltration of T and B cells have significantly prolonged overall survival.[26] In our study, the relative abundance of B cells in subtype B and high-risk score groups with worse OS was lower than that in subtype A and low-risk score groups, suggesting that B cell infiltration inhibits the development of OV. Collectively, our results demonstrated a quantitative and qualitative difference in the landscape of immune infiltration between the distinct pyroptosis subtypes and risk subgroups.

Tumor cells that undergo necroptosis, ferroptosis, and pyroptosis can trigger powerful anti-tumor immunity in vivo and in vitro, and ICIs can synergistically improve their efficacy, even in ICI-resistant tumors.[27] Recently, many studies have focused on immune checkpoint molecules, such as PD-1/PD-L1 and CTLA-4, as components of new strategies for cancer therapy, and found that these molecules can significantly regulate the immune function of TICs.[28,29] Studies have shown that ICIs inhibit tumor development by alleviating the dysfunction of effector T cells. It is traditionally believed that $CD8^+$ T cells activated by immunotherapy induce tumor cell death via two approaches mediated through perforin granzyme and Fas-FasL.[30,31] However, many recent studies have established a new mechanism for $CD8^+$ T cell-mediated inhibition of tumors, by inducing iron death and pyrolysis.[32,33] In the TME, PD-1 on the surface of activated T cells binds to PD-L1 and PD-L2 receptors on the surface of tumor cells, to activate a series of signal factors in immune cells. This process initiates a series of signaling factors in immune cells, to inhibit T cell activation and promote T cell failure, thus helping tumor cells evade immunosurveillance.[34] To date, the use of antibodies that inhibit PD-1 or PD-L1 has achieved moderate results in OV, with a median response rate of 10% to 15%.[35,36] Interestingly, the combination of anti-PD1 nivolumab and anti-CTLA4 ipilimumab showed promising results for platinum-resistant OV, in a six-month interim analysis, with an overall response rate of 34%. Nevertheless, the final results are still awaited for this clinical trial.[37] Moreover, several biological agents have been studied as therapeutic strategies that could be used in combination with PARP inhibitors for immunotherapies, including anti-CTLA-4 and anti-PD-1/PD-L1. The rationale of this treatment is based on the hypothesis that BRCA1/2, and wild-type BRCA1/2 homologous recombination deficient-ovarian tumors display a higher neo-antigen load than homologous recombination-proficient cancers, which in turn produce a more effective anti-tumor immune response.[38] In addition, there is evidence that BRCA deficiency may induce a stimulator of interferon genes-dependent innate immune response, by inducing type-I interferon and pro-inflammatory cytokine production.[39] In addition to OC, a key point of immunotherapy is to find reliable biomarkers for the identification of responders to ICIs. Several biomarkers, such as PD-L1, MSI, and TMB, have a higher level of validation.[40] In this study, we observed higher expression levels of PD-1 and PD-L1 in subtype A and low-risk score groups of OV. TIDE prediction showed that the low-risk group had a significantly lower TIDE score. Moreover, we found that a higher TMB level was observed in the high-risk group, and patients with high TMB had prolonged survival. These findings suggested that patients with low-risk scores have significant therapeutic and clinical benefits.

The signature constructed in the present study contained eight genes, of which five genes (CD44, VSIG4,[41] EPB41L3,[42] IRF4,[43] and ISG20)[44] are closely related to the genesis and development of OV. CD44 is a cell surface glycoprotein that mediates the response of cells to the microenvironment and participates in a variety of intracellular processes, including differentiation, proliferation, and movement.[45] Increasing evidence indicates that CD44 affects the progression of cancer metastasis, maintenance of cancer stem cells, and development of chemoresistance through a variety of mechanisms in a variety of cancers, including OV, and thus, represents a promising therapeutic target for the treatment of OV.[46] There is ample evidence that CD44 and STAT3 act synergistically at multiple levels in the TME, to promote tumor angiogenesis, immunosuppression, and cancer metabolic reprogramming, which is conducive to cancer progression.[47] Zhou et al[48] revealed that high expression of CD44 is significantly correlated with worse prognosis and

promotes OV progression through activation of epithelial-mesenchymal transition, by regulating Snail, ZEB1, and Caveolin-1. VSIG4, a novel B7 family-related macrophage protein, can inhibit T-cell activation. VSIG4 RNA and protein expression levels were found to be higher in OV tissues and associated with the progression and recurrence of OV.[41] Recently, a five-gene signature was built to predict the prognosis of patients with OV.[44] They found that the expression of ISG20 was significantly downregulated and that ISG20 overexpression inhibited the proliferation, migration, and invasion of OV cells and the growth of a xenotransplantation model.

Conclusion

In this study, we revealed global alterations of PRGs at the transcriptional and genetic levels in three types of gynecological cancer and demonstrated the extensive regulatory mechanisms between multi-layer PRG alterations and patient clinicopathological features, prognosis, and TME cell-infiltrating characteristics in OV. These findings highlight the key role of PRG in TME and help develop immunotherapies and promote individualized therapeutic strategies for OV patients.

Abbreviations

TME, tumor microenvironment; PRGs, pyroptosis-related genes; OV, ovarian cancer; PD-L1, programmed death-ligand 1; TIDE, tumor immune dysfunction and exclusion; TMB, lower tumor mutation burden; GSDMD, gasdermin D; CDF, cumulative distribution function; PCA, principal component analysis; DEGs, differentially expressed genes; OS, overall survival; LASSO, least absolute shrinkage and selection operator; ROC, receiver operating characteristics; AUC, area under the curve; ICIs, immune checkpoint inhibitors; ssGSEA, single-sample gene set enrichment analysis; CNV, copy number variation.

Data Sharing Statement

The data supporting all the results of this study are available from TCGA (http://www.cancer.gov/tcga) and GEO (https://www.ncbi.nlm.nih.gov/geo/query/acc.cgi?acc=GSE9891/GSE26712/GSE49997).

Ethics Approval and Consent to Participate

This study was approved by the Ethics Committee of Renmin Hospital of Wuhan University, and all patients provided informed consent. This study was conducted in accordance with the principles of the Declaration of Helsinki.

Author Contributions

All authors made a significant contribution to the work reported, in the conception, study design, execution, acquisition of data, analysis, and interpretation, as well as, in drafting, revising, or critically reviewing the article; gave final approval of the version to be published; have agreed on the journal to which the article has been submitted; and agree to be accountable for all aspects of the work.

Funding

There is no funding to report.

Disclosure

The authors declare that they have no competing interests.

References

1. Kovacs SB, Miao EA. Gasdermins: effectors of pyroptosis. *Trends Cell Biol*. 2017;27(9):673–684. doi:10.1016/j.tcb.2017.05.005
2. Jorgensen I, Miao EA. Pyroptotic cell death defends against intracellular pathogens. *Immunol Rev*. 2015;265(1):130–142. doi:10.1111/imr.12287
3. Rébé C, Derangère V, Ghiringhelli F. Induction of pyroptosis in colon cancer cells by LXRβ. *Mol Cell Oncol*. 2015;Jan-Mar;2(1:e970094. doi:10.4161/23723548.2014.970094
4. Karmakar M, Minns M, Greenberg EN, et al. N-GSDMD trafficking to neutrophil organelles facilitates IL-1β release independently of plasma membrane pores and pyroptosis. *Nat Commun*. 2020;11(1):2212. doi:10.1038/s41467-020-16043-9
5. Gao J, Qiu X, Xi G, et al. Downregulation of GSDMD attenuates tumor proliferation via the intrinsic mitochondrial apoptotic pathway and inhibition of EGFR/Akt signaling and predicts a good prognosis in non-small cell lung cancer. *Oncol Rep*. 2018;40(4):1971–1984. doi:10.3892/or.2018.6634
6. Rogers C, Fernandes-Alnemri T, Mayes L, Alnemri D, Cingolani G, Alnemri ES. Cleavage of DFNA5 by caspase-3 during apoptosis mediates progression to secondary necrotic/pyroptotic cell death. *Nat Commun*. 2017;8:14128. doi:10.1038/ncomms14128
7. Jiang M, Qi L, Li L, Li Y. The caspase-3/GSDME signal pathway as a switch between apoptosis and pyroptosis in cancer. *Cell Death Discovery*. 2020;6:112. doi:10.1038/s41420-020-00349-0
8. Hinshaw DC, Shevde LA. The tumor microenvironment innately modulates cancer progression. *Cancer Res*. 2019;79(18):4557–4566. doi:10.1158/0008-5472.CAN-18-3962
9. Chen F, Zhuang X, Lin L, et al. New horizons in tumor microenvironment biology: challenges and opportunities. *BMC Med*. 2015;5(13):45. doi:10.1186/s12916-015-0278-7
10. Orning P, Lien E, Fitzgerald KA. Gasdermins and their role in immunity and inflammation. *J Exp Med*. 2019;216(11):2453–2465. doi:10.1084/jem.20190545
11. Erkes DA, Cai W, Sanchez IM, et al. Mutant BRAF and MEK inhibitors regulate the tumor immune microenvironment via pyroptosis. *Cancer Discov*. 2020;10(2):254–269. doi:10.1158/2159-8290.CD-19-0672

12. Ye Y, Dai Q, Qi H. A novel defined pyroptosis-related gene signature for predicting the prognosis of ovarian cancer. *Cell Death Discovery*. 2021;7(1):71. doi:10.1038/s41420-021-00451-x
13. Jiang P, Gu S, Pan D, et al. Signatures of T cell dysfunction and exclusion predict cancer immunotherapy response. *Nat Med*. 2018;24 (10):1550–1558. doi:10.1038/s41591-018-0136-1
14. Wang Q, Wang Y, Ding J, et al. A bioorthogonal system reveals antitumour immune function of pyroptosis. *Nature*. 2020;579 (7799):421–426. doi:10.1038/s41586-020-2079-1
15. Tsuchiya K. Switching from apoptosis to pyroptosis: gasdermin-elicited inflammation and antitumor immunity. *Int J Mol Sci*. 2021;22(1):426. doi:10.3390/ijms22010426
16. Kossaï M, Leary A, Scoazec JY, Genestie C. Ovarian cancer: a heterogeneous disease. *Pathobiology*. 2018;85(1–2):41–49. doi:10.1159/000479006
17. Le Saux O, Ray-Coquard I, Labidi-Galy SI. Challenges for immunotherapy for the treatment of platinum resistant ovarian cancer. *Semin Cancer Biol*. 2020;77:127–143. doi:10.1016/j.semcancer.2020.08.017
18. Jiménez-Sánchez A, Memon D, Pourpe S, et al. Heterogeneous tumor-immune microenvironments among differentially growing metastases in an ovarian cancer patient. *Cell*. 2017;170(5):927–38. e20. doi:10.1016/j.cell.2017.07.025
19. Roma-Rodrigues C, Mendes R, Baptista P, Fernandes A. Targeting tumor microenvironment for cancer therapy. *Int J Mol Sci*. 2019;20:4. doi:10.3390/ijms20040840
20. Belli C, Trapani D, Viale G, et al. Targeting the microenvironment in solid tumors. *Cancer Treat Rev*. 2018;65:22–32. doi:10.1016/j.ctrv.2018.02.004
21. Revythis A, Shah S, Kutka M, et al. Unraveling the wide spectrum of melanoma biomarkers. *Diagnostics (Basel, Switzerland)*. 2021;11(8). doi:10.3390/diagnostics11081341.
22. Boussios S, Karathanasi A, Cooke D, et al. PARP inhibitors in ovarian cancer: the route to "Ithaca". *Diagnostics (Basel, Switzerland)*. 2019;9(2):55.
23. Li J, Wang J, Chen R, Bai Y, Lu X. The prognostic value of tumor-infiltrating T lymphocytes in ovarian cancer. *Oncotarget*. 2017;8(9):15621–15631. doi:10.18632/oncotarget.14919
24. Nielsen JS, Sahota RA, Milne K, et al. CD20+ tumor-infiltrating lymphocytes have an atypical CD27- memory phenotype and together with CD8+ T cells promote favorable prognosis in ovarian cancer. *Clin Cancer Res*. 2012;18(12):3281–3292. doi:10.1158/1078-0432.CCR-12-0234
25. Garris CS, Luke JJ. Dendritic cells, the T-cell-inflamed tumor microenvironment, and immunotherapy treatment response. *Clin Cancer Res*. 2020;26(15):3901–3907. doi:10.1158/1078-0432.CCR-19-1321
26. Henriksen JR, Nederby L, Donskov F, et al. Prognostic significance of baseline T cells, B cells and neutrophil-lymphocyte ratio (NLR) in recurrent ovarian cancer treated with chemotherapy. *J Ovarian Res*. 2020;13(1):59. doi:10.1186/s13048-020-00661-4
27. Tang R, Xu J, Zhang B, et al. Ferroptosis, necroptosis, and pyroptosis in anticancer immunity. *J Hematol Oncol*. 2020;13(1):110. doi:10.1186/s13045-020-00946-7
28. Yaghoubi N, Soltani A, Ghazvini K, Hassanian SM, Hashemy SI. PD-1/ PD-L1 blockade as a novel treatment for colorectal cancer. *Biomed Pharmacother*. 2019;110:312–318. doi:10.1016/j.biopha.2018.11.105
29. Rotte A. Combination of CTLA-4 and PD-1 blockers for treatment of cancer. *J Exp Clin Cancer Res*. 2019;38(1):255. doi:10.1186/s13046-019-1259-z
30. Nguyen LT, Ohashi PS. Clinical blockade of PD1 and LAG3–potential mechanisms of action. *Nat Rev Immunol*. 2015;15(1):45–56. doi:10.1038/nri3790
31. Sun C, Mezzadra R, Schumacher TN. Regulation and function of the PD-L1 checkpoint. *Immunity*. 2018;48(3):434–452. doi:10.1016/j.immuni.2018.03.014
32. Zhang Z, Zhang Y, Xia S, et al. Gasdermin E suppresses tumour growth by activating anti-tumour immunity. *Nature*. 2020;579 (7799):415–420. doi:10.1038/s41586-020-2071-9
33. Wang W, Green M, Choi JE, et al. CD8(+) T cells regulate tumour ferroptosis during cancer immunotherapy. *Nature*. 2019;569 (7755):270–274. doi:10.1038/s41586-019-1170-y
34. Ai L. Xu A and Xu J. Roles of PD-1/PD-L1 pathway: signaling, cancer, and beyond. *Adv Exp Med Biol*. 2020;1248:33–59.
35. Sato E, Olson SH, Ahn J, et al. Intraepithelial CD8+ tumor-infiltrating lymphocytes and a high CD8+/regulatory T cell ratio are associated with favorable prognosis in ovarian cancer. *Proc Natl Acad Sci U S A*. 2005;102(51):18538–18543. doi:10.1073/pnas.0509182102
36. González-Martín A, Sánchez-Lorenzo L. Immunotherapy with checkpoint inhibitors in patients with ovarian cancer: still promising? *Cancer*. 2019;125(Suppl 24):4616–4622. doi:10.1002/cncr.32520
37. Zamarin D, Burger RA, Sill MW, et al. Randomized Phase II trial of nivolumab versus nivolumab and ipilimumab for recurrent or persistent ovarian cancer: an NRG oncology study. *J Clin Oncol*. 2020;38 (16):1814–1823. doi:10.1200/JCO.19.02059
38. Strickland KC, Howitt BE, Shukla SA, et al. Association and prognostic significance of BRCA1/2-mutation status with neoantigen load, number of tumor-infiltrating lymphocytes and expression of PD-1/PD-L1 in high grade serous ovarian cancer. *Oncotarget*. 2016;7(12):13587–13598. doi:10.18632/oncotarget.7277
39. Boussios S, Karihtala P, Moschetta M, et al. Combined strategies with Poly (ADP-Ribose) Polymerase (PARP) Inhibitors for the treatment of ovarian cancer: a literature review. *Diagnostics (Basel, Switzerland)*. 2019;9(3):5.
40. Lu S, Stein JE, Rimm DL, et al. Comparison of biomarker modalities for predicting response to PD-1/PD-L1 checkpoint blockade: a systematic review and meta-analysis. *JAMA Oncol*. 2019;5 (8):1195–1204. doi:10.1001/jamaoncol.2019.1549
41. Byun JM, Jeong DH, Choi IH, et al. The significance of VSIG4 expression in ovarian cancer. *Int J Gynecol Cancer*. 2017;27 (5):872–878. doi:10.1097/IGC.0000000000000979
42. Dafou D, Grun B, Sinclair J, et al. Microcell-mediated chromosome transfer identifies EPB41L3 as a functional suppressor of epithelial ovarian cancers. *Neoplasia (New York, NY)*. 2010;12(7):579–589. doi:10.1593/neo.10340
43. Heimes AS, Schmidt M, Jäkel J, et al. A retrospective analysis of immunohistochemically determined IRF4 (interferon regulating factor 4) expression in a consecutive cohort of 114 ovarian cancer patients. *Arch Gynecol Obstet*. 2019;299(1):239–246. doi:10.1007/s00404-018-4941-z
44. Yu J, Liu TT, Liang LL, et al. Identification and validation of a novel glycolysis-related gene signature for predicting the prognosis in ovarian cancer. *Cancer Cell Int*. 2021;21(1):353. doi:10.1186/s12935-021-02045-0
45. Ponta H, Sherman L, Herrlich PA. CD44: from adhesion molecules to signalling regulators. *Nat Rev Mol Cell Biol*. 2003;4(1):33–45. doi:10.1038/nrm1004
46. Martincuks A, Li PC, Zhao Q, et al. CD44 in ovarian cancer progression and therapy resistance-A critical role for STAT3. *Front Oncol*. 2020;10:589601. doi:10.3389/fonc.2020.589601
47. Jiang YX, Siu MK, Wang JJ, et al. Ascites-derived ALDH+CD44+ tumour cell subsets endow stemness, metastasis and metabolic switch via PDK4-mediated STAT3/AKT/NF-κB/IL-8 signalling in ovarian cancer. *Br J Cancer*. 2020;123(2):275–287. doi:10.1038/s41416-020-0865-z
48. Zhou J, Du Y, Lu Y, et al. CD44 expression predicts prognosis of ovarian cancer patients through promoting Epithelial-Mesenchymal Transition (EMT) by regulating snail, ZEB1, and Caveolin-1. *Front Oncol*. 2019;9:802. doi:10.3389/fonc.2019.00802